Validation of the 50 GHz sea ice emissivity product

OSI-404-a

Version: 1.6

Date: 01/05/2018

Rasmus T. Tonboe, John Lavelle, Eva Howe, Harald Schyberg, Frank T. Tveter

Document Change record

Document version	Software version	Date	Author	Change description
1.0		12.12.11	HS	First version of methods and results
1.1		05.07.13	HS	Revisions after review, including extended validation period
1.2		20.12.13	RT	Minor changes after close-out review
1.3		29.02.16	RT	Addition of Chapter 8 on continuous validation and conclusions in Chapter 9
1.4		09.05.16	RT+ JOL	Minor changes after close-out review
1.5		26.09.2016	EH	Minor changes after update of requirements
1,6 draft		14.12.17	RT	Revisions before OSI-404-a operations readiness review, including extended validation period
1.6		01.05.18	RT, JOL	Minor changes after OSI-404-a ORR.

Table of contents

1. Introduction

1.1. Scope

The purpose of this report is to describe the validation of the OSI SAF near 50 GHz sea ice emissivity product.

The quality assessment of the OSI SAF sea ice emissivity product (OSI-404) is done first just before becoming an operational/pre-operational product distributed by the OSI SAF. This first assessment is explained in this scientific validation report. Then continuous monitoring of the product quality is done by the OSI SAF team and presented in the half-yearly operations reports available on the OSI SAF web site project documentation.

The quality assessment of the OSI SAF sea ice emissivity product (OSI-404) is done against the target accuracy requirement defined in the OSI SAF Service Specification [RD.12].

The target accuracy corresponds to the desired performance level (the breakthrough accuracy). If the values are not compliant to the target accuracy requirement, we consider that the product is still useful/useable as long as the values are compliant to the threshold requirement.

Target accuracy: 5% (yearly average)

Threshold accuracy: 15% (yearly average)

1.2. Glossary

Acronym	Description
AMSU	Advanced Microwave Sounding Unit
ATBD	Algorithm Theoretical Basis Document
DMI	Danish Meteorological Institute
OSI SAF	Ocean and Sea Ice SAF
HIRLAM	High-Resolution Limited Area Model
METNO	Norwegian Meteorological Institute
MY	Multi Year (sea ice)
NOAA	National Oceanic and Atmospheric Administration
NWP	Numerical Weather Prediction
PUM	Product User Manual
RTTOV	Radiative Transfer model for TOVS
SAF	Satellite Application Facility
SSM/I	Special Sensor Microwave Imager
SSMIS	Special Sensor Microwave Imager/Sounder
TBC	To Be Confirmed
TBD	To Be Determined
TBW	To Be Written

1.3. Reference documents

[RD.1] Tonboe, R.T. and H. Schyberg, 2011: Algorithm theoretical basis document for the OSI SAF 50GHz sea ice emissivity model. Ocean and Sea Ice SAF document OSI-404.

[RD.2] Heygster, G., C. Melsheimer, N. Mathew, L. Toudal, R. Saldo, S. Andersen, R. Tonboe, H. Schyberg, F. Thomas Tveter, V. Thyness, N. Gustafsson, T. Landelius, and P. Dahlgren. 2009. POLAR PROGRAM: Integrated Observation and Modeling of the arctic Sea Ice and Atmosphere. Bulletin of the American Meteorological Society 90, 293 – 297.

[RD.3] Tonboe, R. T., E. Nielsen, R. Larsen, 2011: Product Users Manual for the OSI SAF 50GHz sea ice emissivity product. Ocean and Sea Ice SAF document OSI-404.

[RD.4] Mathew et al, 2008: Surface Emissivity of Arctic Sea Ice at AMSU Window Frequencies. IEEE Transactions on Geoscience and Remote Sensing, Vol. 46, no.8, pp. 2298-2306.

[RD.5] Kongoli et al, 2011: A New Sea-Ice Concentration Algorithm Based on Microwave Surface Emissivities—Application to AMSU Measurements.
IEEE transactions on Geoscience and Remote Sensing, Vol 49, issue 1, pp 175 - 189.

[RD.6] Ocean and Sea Ice SAF CDOP Product Requirement Document, v2.4.

[RD.7] Karbou, F., E. Gérard, and F. Rabier, 2006, Microwave Land Emissivity and Skin Temperature for AMSU-A & -B Assimilation Over Land, Q. J. R. Meteorol. Soc., vol. 132, No. 620, Part A, pp. 2333-2355(23).

[RD.8] Tonboe, R. T., H. Schyberg, E. Nielsen, K. R. Larsen, F. T. Tveter. The EUMETSAT OSI SAF near 50 GHz sea ice emissivity model. Tellus A, 2013, 65, 18380, http://dx.doi.org/10.3402/tellusa.v65i0.18380.

[RD.9] Wentz, F. J. and T. Meissner, (2000), AMSR Ocean Algorithm, Version 2, report number 121599A-1, Remote Sensing Systems, Santa Rosa, CA, 66pp.

[RD.10] Users guide to the ECMWF forecast products, v1.2, 2015. (http://www.ecmwf.int/sites/default/files/User_Guide_V1.2_20151123.pdf)

[RD.11] OSI SAF; *CDOP 3 Product Requirement Document (PRD)*

SAF/OSI/CDOP3/MF/MGT/PL/2-001, Version 1.1, 20/11/2017

[RD.12] OSI SAF; *Service Specification (SeSp)*

SAF/OSI/CDOP3/MF/MGT/PL/003, Version 1.3, 14/12/2017

Reference to a Reference Document within the body of this document is indicated as reference in the list above, e.g. [RD.1].

1.4. Eumetsat Disclaimer

2. Background

In the OSI SAF a microwave sea ice emissivity product has been developed and implemented. To perform atmospheric sounding using microwave remote sensing over sea ice, it is necessary to take into account the surface contribution of the signal, which is determined by emissivity together with surface effective temperature.

This product is intended for supporting microwave temperature sounding of the atmosphere using the oxygen absorption lines near the 50 GHz microwave channels on microwave radiometers such as AMSU (Advanced Microwave Sounding Unit) and SSMIS (Special Sensor Microwave Imager/Sounder), for instance by data assimilation in numerical weather prediction (NWP) models. The assumption is that sea ice emissivity in most parts of the Arctic has relatively stationary properties in time, so that daily derived emissivities also are meaningful as estimates of the actual emissivity for a short time range into the future. The brightness temperature measurements required as input to the emissivity model are collected from the microwave conically scanning imagers SSM/I and SSMIS data using a similar gridding approach as for instance the OSI SAF ice concentration product.

Details on the approach for deriving the emissivity is found in the algorithm theoretical basis document (ATBD) [RD.1] and the product users manual (PUM) [RD.3]. The product consists of fields on the OSI SAF grid of two parameters in an emissivity model describing the surface, denoted "R" and "S" in the ATBD. When these parameters are available, the emissivity for a specified observation geometry and polarization, for instance that for the AMSU instruments, can be easily computed from the mathematical relations described in the ATBD and PUM, for instance in a simple subroutine. It should be noted that only the two local parameters "R" and "S" are determined and updated dynamically in the form of geographical grids which are regularly updated and delivered by the OSI SAF. This is sufficient for determining the emissivity for a certain observation geometry. For further details and formulae, see Section 8 of the ATBD.

This report describes the validation undertaken for the emissivity product. The validation approach is described in the next section and is done by using the emissivity product to simulate AMSU-A observations from the NOAA satellites and evaluating the fit to real AMSU-A observations.

3. Validation approach

Validation can in general be performed by comparison with independent observations of the quantity of interest. In this case only very few *in sit* data-sets of the sea ice emissivity exists, mainly data from campaigns which are not easily accessible. In addition, such measurements have representativeness issues, as they only measure at points or limited areas and not the full foot-print coverage. Threshold and target accuracies for the OSI SAF emissivity product of 0.15 and 0.05 (absolute values, since emissivity is a dimension less quantity) respectively are defined in the Product Requirements Document [RD.6], however the lack of measurements and available methodology makes it problematic to objectively determine the accuracy of the product.

Since we target 50 GHz sounding for this emissivity product, we have chosen to study the fit that we can obtain with this emissivity product when using it to simulate the lower tropospheric AMSU-A channels which are sensitive to the surface contribution from the sea ice. Since helping to simulate the surface contribution to the sounding channels is a main target of the emissivity product, the ability of the product to produce a good fit to such observations in these forward calculations is seen as a good indicator of the suitability of the product.

However, forward simulations also uses other information. The emissivity product together with the effective surface temperature is used as input to the RTTOV radiative transfer model, which then simulates the effect on the radiation of the further path through the atmosphere. This simulation relies on a surface temperature estimate and atmospheric temperature and moisture profiles, which we will take from the HIRLAM NWP model of met.no.

This means that errors and problems related to the atmospheric profiles and, probably even more important, the surface temperature, affects the comparison and the fit between simulated and real observations.

Model simulations indicate that the snow-ice interface temperature or alternatively the 6 GHz brightness temperature is a closer proxy for the 50 GHz effective temperature than the snow surface or air temperature.

In the comparison several factors can cause differences between the output of the forward simulations and the observations:

1. Errors in the observations themselves
2. Mismatch in time and space averaging between observation footprint and the model representation of it, referred to as representativeness error
3. Errors in the HIRLAM atmospheric profiles and surface temperatures
4. Errors in the emissivity input to the forward simulation
5. Errors in the forward model itself

The basic hypothesis which we wish to use for the analysis is that when we only change the emissivity estimate and keep the other factors constant, a better fit indicates a more accurate emissivity estimate, and we can take the fit as an indication of the quality of the estimate. Even if a first guess would be that the various errors listed are not correlated, there is a risk of anti-correlated, compensating errors. Theoretically an increased error in the emissivity estimate can compensate for an error in one of the other factors of opposite sign. If this is the case, our assumption that a better fit represents a better emissivity estimate might break down.

We do not have, however, any reason to expect any such anti-correlation between emissivity changes

and the other factors in question, so it is very likely that the fit is a good indicator of the accurateness of emissivity estimate in our analysis.

4. Data sets

The statistics to be presented here is based on OSI SAF emissivity data, HIRLAM model data and AMSU-A observations spanning two time periods in the autumn of 2011 and later using the continuous validation also the more recent 2015 and 2017. It does not span a full yearly sea ice cycle, which is a limitation, but still covers a large Arctic area with sea ice of different properties and time variations.

The climatology of emissivity development for the near 50 GHz channels throughout the year in the Arctic is different for first-year and multi-year sea ice (see for instance Mathew et al, 2008). First-year emissivities have high values early in the year, gradually decreasing throughout the spring, and minimum values during the summer melt season. From August-September during the freeze-up until November-December, there is a strong increase in first-year emissivity. Multi-year emissivities have relatively stable values early in the year, with a slight increase before a pronounced maximum in the melt season, then a gradual decrease again throughout the autumn.

By doing our validation in the freeze-up season with its substantial trends in evolution of the sea ice properties and emissivities as described above, the dataset will comprise a range of emissivities and conditions, although spring and summer melt conditions are missing from the dataset. To check the robustness and variability of the statistical results to be presented, we have performed validation on two different time periods, the first from 19 October to 30 November 2011 and the second partly overlapping from 1 November to 31 December 2011. The figures and statistical measures were very similar in both periods and supported identical conclusions from the two datasets.

The OSI SAF production chain has been set up and has produced grids of the R and S parameters of the emissivity model for a time period which includes the above periods. Also the necessary HIRLAM fields have been stored for the same time periods.

HIRLAM is a state-of-the-art hydrostatic NWP model, and the version applied here has 12 km horizontal resolution. This is the main operational regional NWP model of met.no. Its domain is shown in Fig. 1, and covers a large part of the Arctic ice cap. HIRLAM is updated with assimilation of new observations with a 3D-Var scheme every 6 hours.

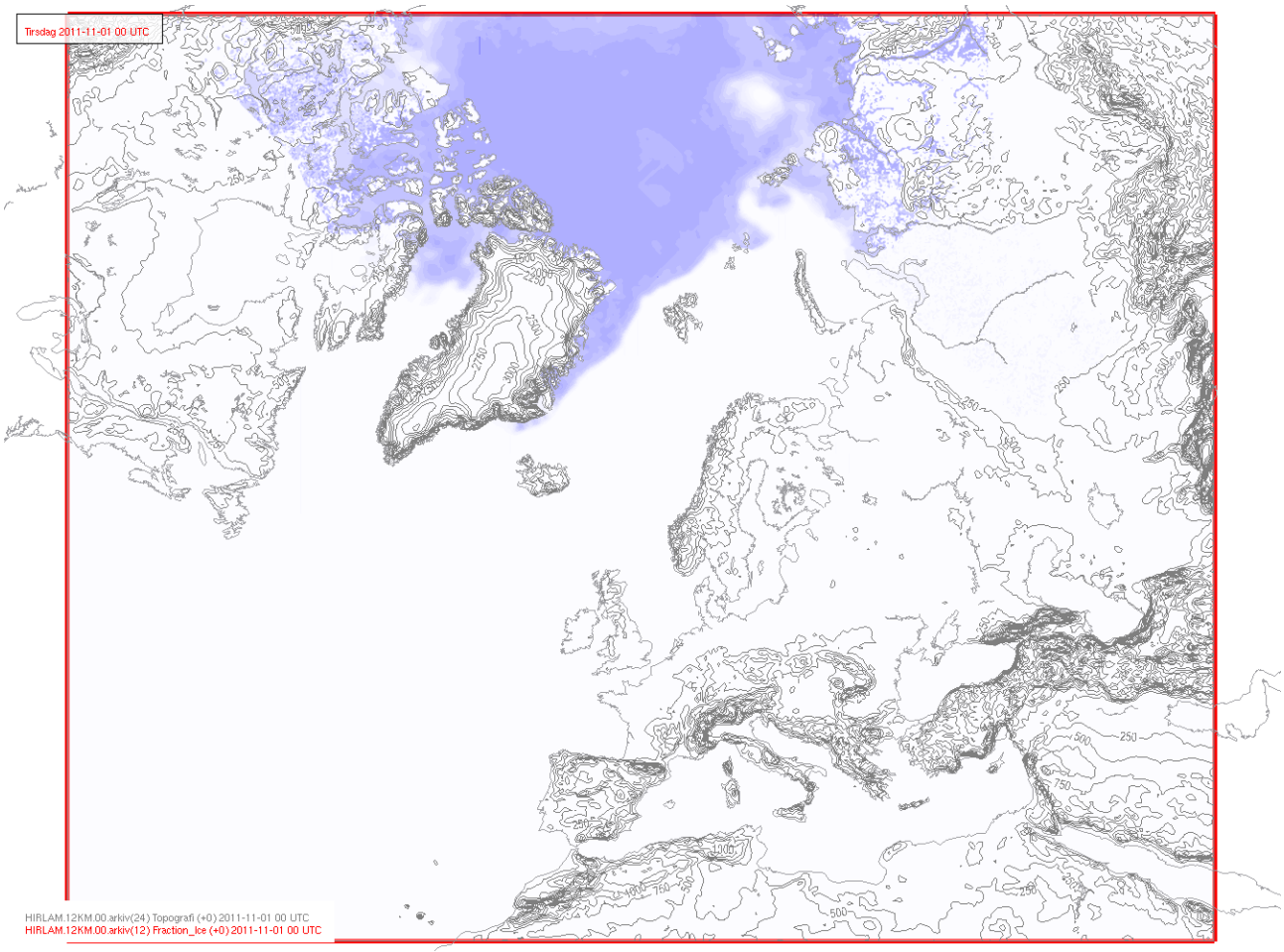

Figure 1: The domain of the HIRLAM 12 km model from which the meteorological data at the AMSU footprints are taken. The sea ice coverage on 1 November 2011 is indicated with blue shading. (Contours are coasts and surface topography.)

For this validation study, all AMSU-A brightness temperature data from the NOAA-15 and NOAA-16 satellites within the HIRLAM domain in the above time period have been collected. For each AMSU-A footprint, HIRLAM data have been collocated. The HIRLAM short-range forecasts at between 6 and 12 hours lead time, have been interpolated in time to the exact time of each AMSU observation. Also, the HIRLAM data have been averaged over each AMSU footprint.

HIRLAM assimilates AMSU-A observations, but not over sea ice where the validation is done. The data used for validation are short-range forecasts and not analyses, so the effect of observations on the atmospheric state has propagated through the model integration and is also influenced by boundaries and model physics (and also by all other observation types). Because of this there will be no "incest" problems in the validation, although AMSU-A observations have been used by the model.

The actual AMSU-A incidence angle and its polarization mix has been used in the emissivity model provided in the ATBD, to give emissivities at the actual AMSU-A footprints. Since one AMSU-A footprint covers many OSI SAF grid points, the values were averaged over each AMSU footprint.

As for the AMSU data, we are interested in the observations where the surface has an influence. The AMSU brightness temperatures can be shown from radiative transfer theory to be functions of the temperature averaged over deep layers in the atmosphere with some averaging kernel or weighting function. The weighting functions are only changing very little with atmospheric state. Typical weighting functions for the AMSU-A channels are shown in Fig. 2. We see that channels 3 and 4 are mainly surface channels, while the channels above have a peak in the atmosphere and can be used for atmospheric sounding. Channels 5, 6 and 7 have obvious surface contributions, decreasing in magnitude, while channel 8 and the above channels have weighting functions entirely above the surface.

To select data over sea ice for the analysis, and ensure that possible contamination from for instance open water surface in the footprints is negligible, we have only considered those satellite footprints where the sea ice concentration exceeds 95%. The concentration used for this criterion is taken from the daily OSI SAF sea ice concentration product. No screening for data contaminated by clouds has been done.

For each AMSU-A observation point, the OSI SAF emissivity product together with HIRLAM surface temperatures and temperature and moisture profiles have been used as input to the radiative transfer model RTTOV-8 to simulate brightness temperatures for comparison with the real observed AMSU-A data. This has been repeated with alternative formulations for the sea ice emissivity for comparison.

The AMSU-A data amount obtained in the dataset is very large, so for scatter plots presented in the report, points have been removed by a thinning procedure for practical plotting purposes.

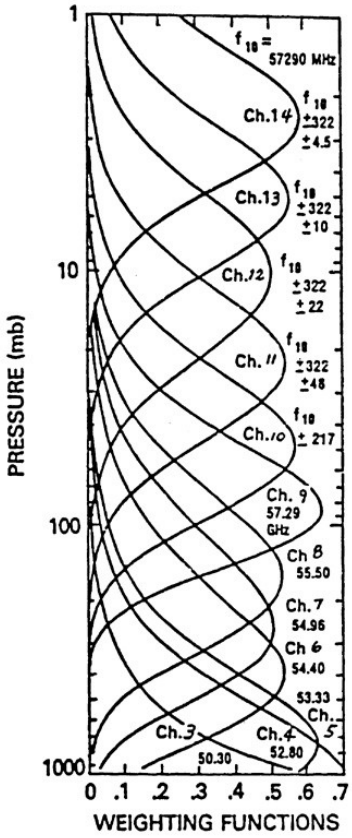

Figure 2: Typical weighting functions as a function of pressure (vertical axis) for the AMSU-A channels. (From "AMSU-A instument guide" at NASA website.)

5. Comparison of emissivities applying various approaches

We have compared the emissivities with the OSI SAF method with those from the method outlined in [RD.2], where emissivities is proposed to be expressed as a linear function of the retrieved multi-year sea ice fraction, ranging from 0.796 in areas of pure multi-year-ice to 0.928 for pure first-year ice. The multi-year fraction is estimated implicitly in the OSI SAF sea ice concentration algorithm, again based on SSMI or SSMIS data. This multi-year (MY) concentration estimate has been output and stored in gridded form for use in this alternative emissivity estimate. The comparison of these two emissivity data sets are shown in Fig. 3.

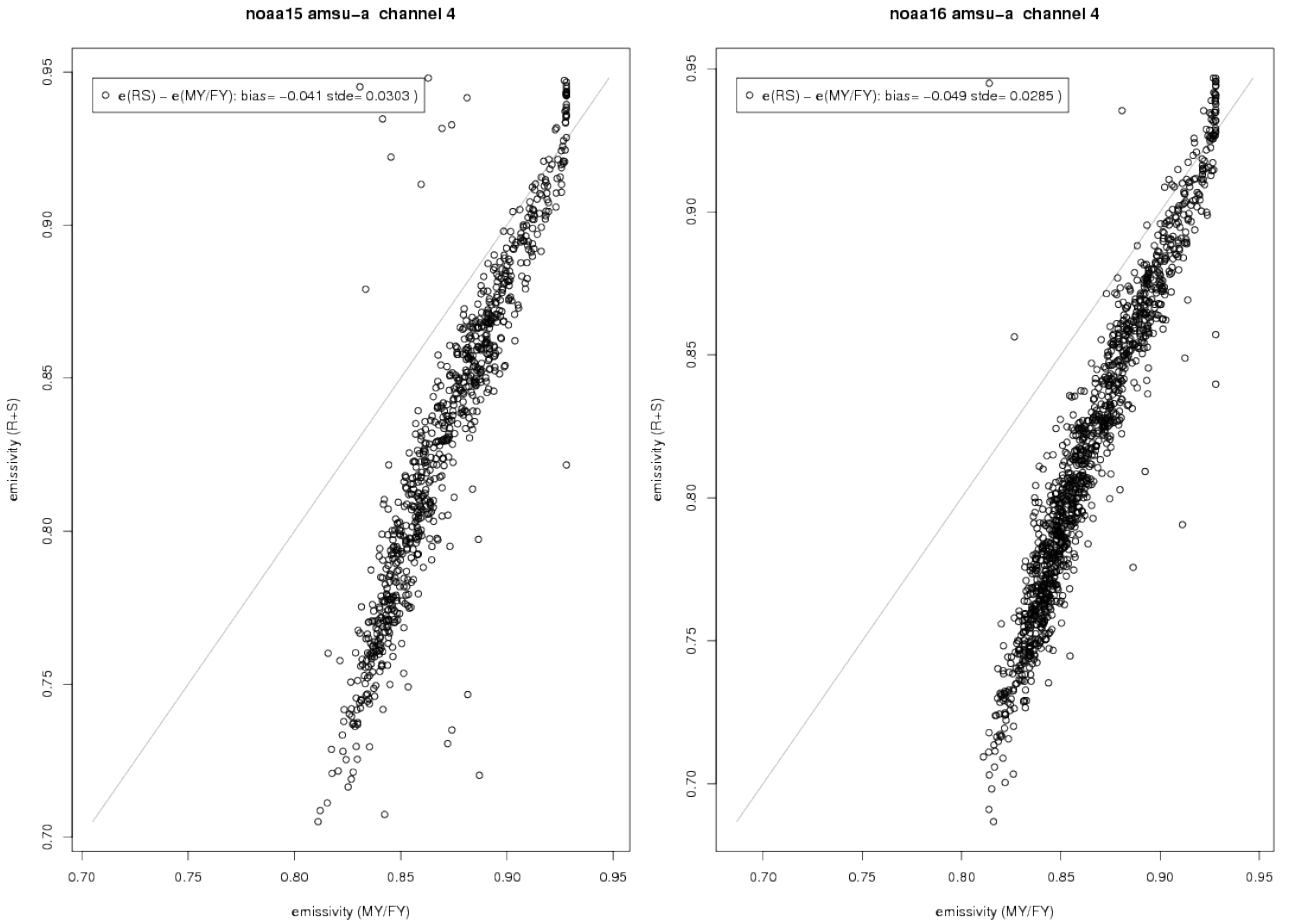

Figure 3: Comparison between emissivities calculated using the MY fraction (horizontal axis) and using the OSI SAF product (vertical axis). Data is for the period 19 Oct to 30 Nov 2011. Left: Dataset from NOAA-15. Right: From NOAA-16

There is a strong correlation between the emissivities found with the two methods. Both the OSI SAF "R+S" method and the MY methods captures most variability from a strong 19-37GHz gradient ratio (GR1937) dependence, but the R+S method has a larger "dynamic range". In the comparison between the MY and the R and S method the slope is greater than one. There are large differences for the multi-

year ice, while both models agree for first-year. The MY based emissivities are constrained by the tie-points while the R and S emissivities are unconstrained and varies primarily as a function of the spectral gradient ratio. Adjusting the MY method multi-year ice tie-point could minimize the bias between the methods.

The two methods seem to agree on the first-year-ice emissivities, which for both methods are around 0.92 for pure first-year-ice. For pure multi-year ice, the R+S method lies around 0.7 while the MY fraction based method is around 0.8. Estimates of Arctic multi-year emissivities are also given in literature. Mathew et al [RD.4] indicates MY ice emissivity values in November between 0.6 and 0.8 depending on incidence angle. That paper also compares their emissivity estimates with previous literature, and it seems to indicate typical emissivity values closer to that found for the R+S product than in the MY product. Kongoli et al [RD.5] indicates typical emissivity values in the Arctic of 0.73, also closer to the R+S method.

We have also investigated the fit between the two emissivity estimates for each incidence angle (scatter plots not shown). While the slope of the relation between the emissivity estimates varies with incidence angle, there is still scatter between the two emissivities for each incidence angle, showing that even after removing the degree of freedom from incidence angle, there is still variability left, since the R+S method is a two-parameter model and has more freedom than the MY based method, depending only on one scalar describing the surface.

In general the differences found between the R+S method and the MY based method are as expected, but there seems to be more physical realism in the R+S based method. In addition we have also compared the R+S OSI SAF emissivity product to the so called "dynamical method" for estimating emissivities from a surface channel of the AMSU-A sounding data.

The dynamical method can be derived from a simplified radiative transfer equation, and is based on simulating the brightness temperatures with RTTOV at zero and one emissivities, $T_{b\ sim}(\varepsilon=0)$ and $T_{b\ sim}(\varepsilon=1)$ and using that together with the real observed brightness temperature, $T_{b\ obs}$,

$$\varepsilon = (T_{b\ obs} - T_{b\ sim}(\varepsilon=0)) \ / (T_{b\ sim}(\varepsilon=1) - T_{b\ sim}(\varepsilon=0)) \qquad \text{(eq. 1)}$$

The method is for instance described and applied in Mathew et al [RD.4], and is based on determining the emissivity so that the misfit between observed and simulated observations in the chosen channel disappears. In our case we have used AMSU-A channel 3, which is a surface channel in the 50GHz region, to determine the emissivity. It is generally accepted that emissivity varies slowly with frequency over sea ice, so this emissivity should then also serve as a good estimate in the nearby 50 GHz sounding channels. The method has also been applied by Karbou when using microwave sounding data over land in data assimilation, see for instance Karbou et al [RD.7].

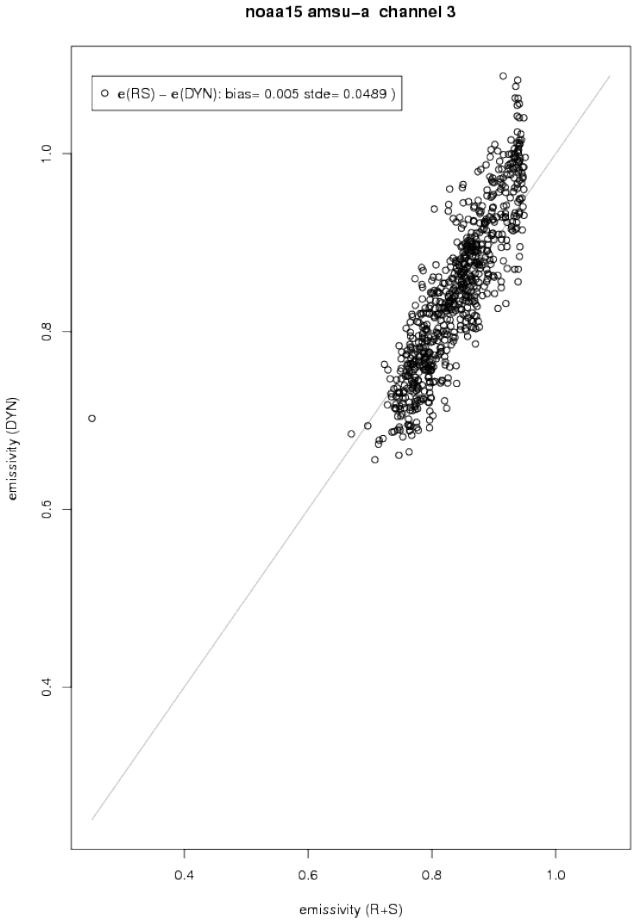

Figure 4: Comparison between emissivities calculated using the OSI SAF product and "dynamical" emissivities based on channel 3 (vertical axis). Dataset from NOAA-15 for the period 19 Oct to 30 Nov 2011.

Figures 4 and 5 show the dynamical emissivities versus the OSI SAF emissivities for the AMSU-A footprints of NOAA-15 and NOAA-16 respectively. On average we find a good correspondence between the two emissivity estimates, although the scatter between the two methods is relatively large, larger than when comparing the R and S method to the MY based emissivity estimates. In general the scatter between the R+S and dynamical estimates is slightly larger at high emissivities (typical for first-year ice). There is nothing in the mathematical expression for the dynamical emissivity which forces it to be within the physical meaningful range below unity, and values larger than one are seen. It should be noted that the way the dynamical emissivity is derived, there is a risk that observation errors, atmospheric signals (even in channel 3 some atmospheric contribution is found) or errors in the surface temperature or profiles entering RTTOV are falsely used to adjust the dynamical emissivity. There seems to be a tendency that the average dynamical emissivity are slightly higher at high emissivities.

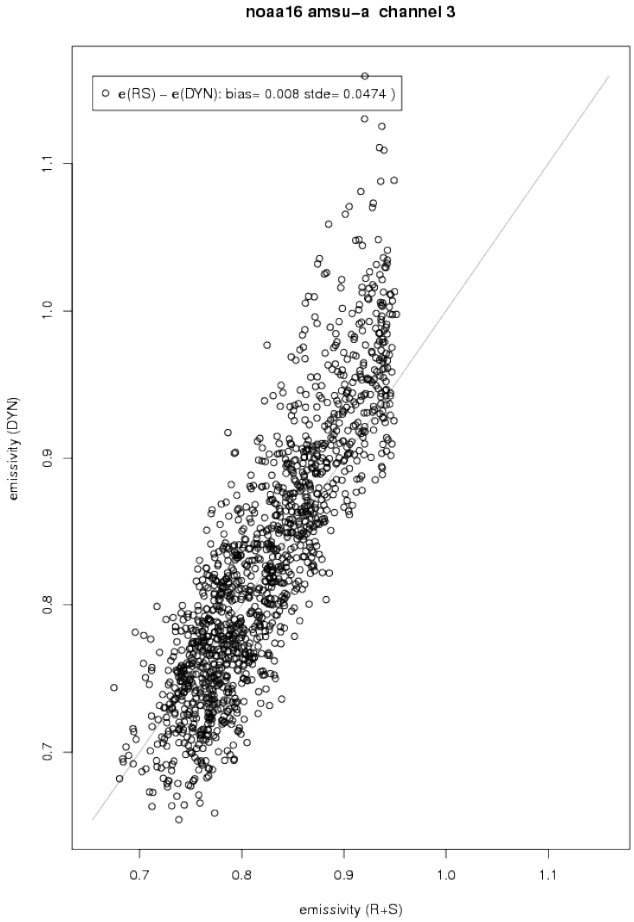

Figure 5: Comparison between emissivities calculated using the OSI SAF product and "dynamical" emissivities based on channel 3 (vertical axis). Dataset from NOAA-16 for the period 19 Oct to 30 Nov 2011.

6. Fit of simulated data to observations using the emissivities

We will here validate the emissivity product in the context of using the emissivity in a forward radiative transfer calculation to estimate sounding channel brightness temperature. This is in line with how sounding channels are used in NWP data assimilation, where variational methods are usually applied with only forward calculations. The assimilation methods adjust the atmospheric state to give a best possible simultaneous fit to all information, including the observations.

The dataset and preprocessing used in studying this fit has been described above. For as meaningful validation as possible we are interested in removing as many other sources to scatter and errors as possible, other than the surface emissivities. All weather centres assimilating sounding data recognize that there are systematic errors in the observations and the forward model (radiative transfer model such as RTTOV) describing the observations, which can partly be removed by a bias correction procedure. The bias correction uses standard statistical regression on a dataset of observations and corresponding simulated observations to find an optimal correction to the observations. This correction has a constant term and also applies a small set of predictors assumed to influence the errors.

The bias correction needs forward calculations already assuming an emissivity model. We first tried to compare the match between observed and simulated brightness temperatures without any bias correction. It turned out to produce quite large scatter, which could be expected, making it difficult to interpret the results. We have therefore chosen to implement the bias correction scheme used in data assimilation to correct the observations before studying the fit.

A particular problem and source of error over sea ice is the definition of the emitting surface temperature. The standard data we have available to present to RTTOV is the ice surface temperature from HIRLAM. However the microwave channels studied here have some penetration depth below surface. Since temperature is usually increasing with depth in the sea ice, the efficient emitting temperature is often higher than the HIRLAM surface temperature, and it is important to deal with this issue if we want to assess effects of altering surface emissivities.

Mathew et al [RD.4] finds a linear relation $T_{em}= a*T_{air} + b$ between efficient emitting temperature and surface air temperature, where the relation can be found by a standard linear regression. Alternatively it has been proposed to use the temperature at the snow-ice-interface as emitting temperature rather than the top-of-snow surface temperature. This would lead to a similar linear relation. In our case we can obtain the same effect by including the surface temperature as a predictor in the bias correction. The relation between changes in surface emitting temperature and changes in satellite brightness temperatures turns out to be quite linear, so including the surface temperature as a predictor will yield a correction which describes the appropriate correction, with linear coefficients determined implicitly from the dataset rather than being pre-determined.

In addition to surface temperature, scan angle, scan angle squared and thickness (vertically averaged temperature) of several atmospheric layers were used as predictors in the bias correction. We have determined separate bias correction coefficients for the observations for the OSI SAF R+S emissivity product and for the MY based emissivity estimate.

When investigating the fit between simulated and real observations for the dynamical emissivity method, we have not done a separate bias correction, but used the bias coefficients from the R+S emissivity dataset. This is because we expect that a prior bias correction would make the emissivity

derived with the dynamical method from AMSU channel 3 (50.3GHz) more physically realistic, since it would take away some of the error sources connected to the observations described in Section 3. Previous applications of the dynamical method have derived emissivities from non-bias-corrected observations. Fig 11 shows a comparison of dynamic emissivities calculated with non-bias-corrected and bias-corrected observations. We see that there are significant differences between the two emissivity estimates and that the bias correction largely reduces the number of non-physical emissivities above one.

We have also tested the effect of the two different dynamic emissivity estimates (with and without bias corrected brightness temperatures) on the comparison between simulated and observed brightness temperatures. In Figures 12 and 13 we show simulated vs. observed AMSU-A data in channel 5 for dynamic emissivities from non-bias-corrected and bias-corrected data respectively. We clearly see that a better fit to the observations is obtained using bias corrected data for the dynamical emissivities, and in Fig. 10 we show results from the dynamical method based on bias corrected data only.

Figures 6-9 show the fit between simulated and observed NOAA-15 AMSU-A brightness temperatures for channels 4-7 respectively. The scatter plots show the fit both for the MY based emissivity method and the OSI SAF R+S method. Channel 4 is mainly a surface channel, and has largest scatter and worst fit between observed and simulated values, reflecting the fact that there is a significant uncertainty in determining the surface contribution to the signal. For channels 5-7 which are atmospheric channels with gradually decreasing surface contribution, this is reflected in that the fit between simulated and observed becomes gradually better with less surface contribution. Generally we seem to obtain a better fit with the OSI SAF R+S method than with the MY based method.

We have also done the same analysis for NOAA-16. Scatter plots are not shown here, but the results are qualitatively the same. In addition the same analyses was performed for a shifted time period covering 1 November – 31 December (instead of 19 October - 30 November) with qualitatively the same results (not shown here).

The datasets in the plots presented in Figs. 6-9 includes all AMSU-A incidence angles in the dataset. We have also investigated similar plots for each incidence angle bin (not shown here). The deviations and scatter did not show any systematic changes related to incidence angle.

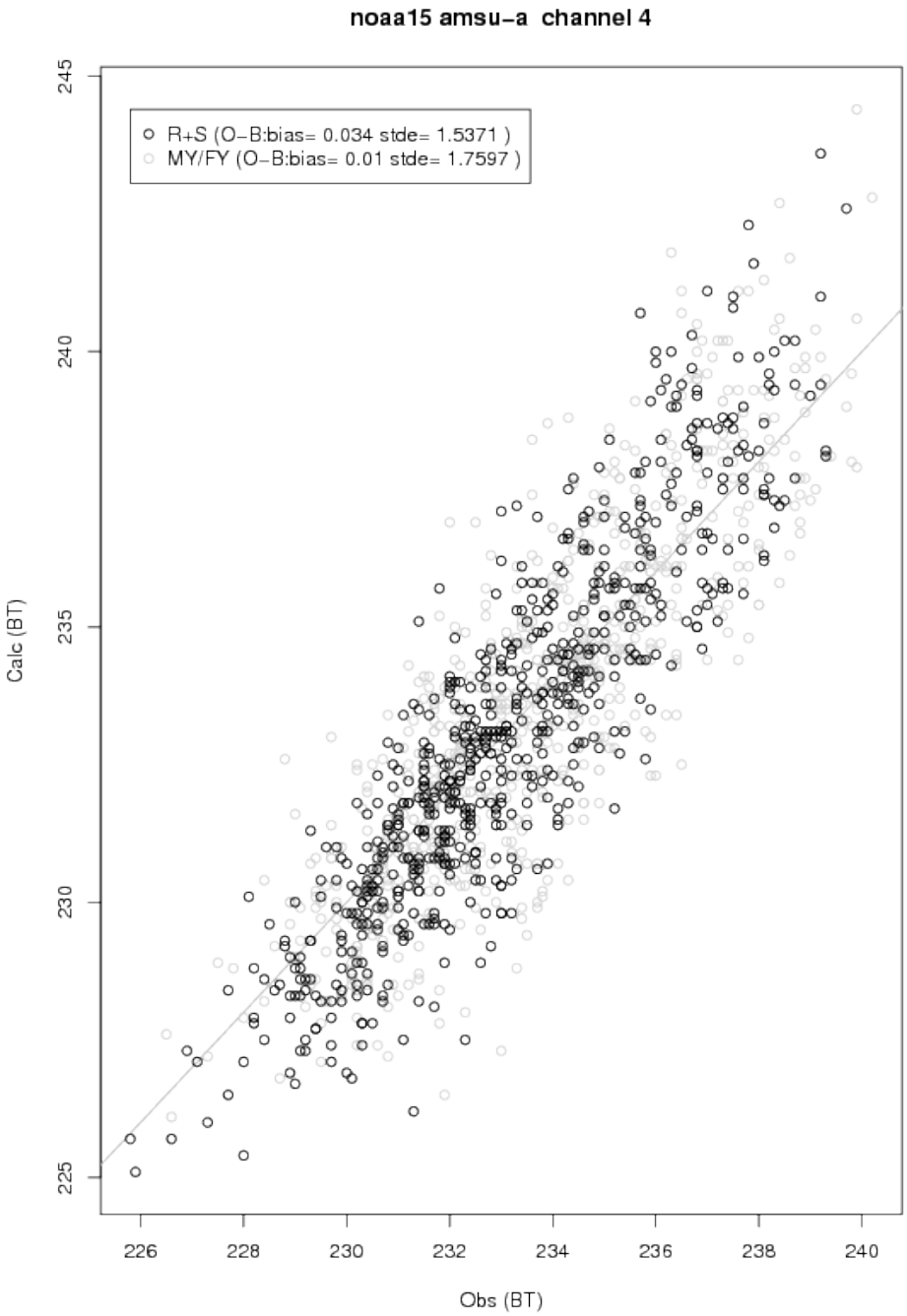

Figure 6: Observed (bias corrected) vs. simulated AMSU-A channel 4 brightness temperatures using the two approaches for emissivities: R+S (OSI SAF) and MY/FY (Heygster et al in [RD.2]). Data is for the period 19 Oct to 30 Nov 2011.

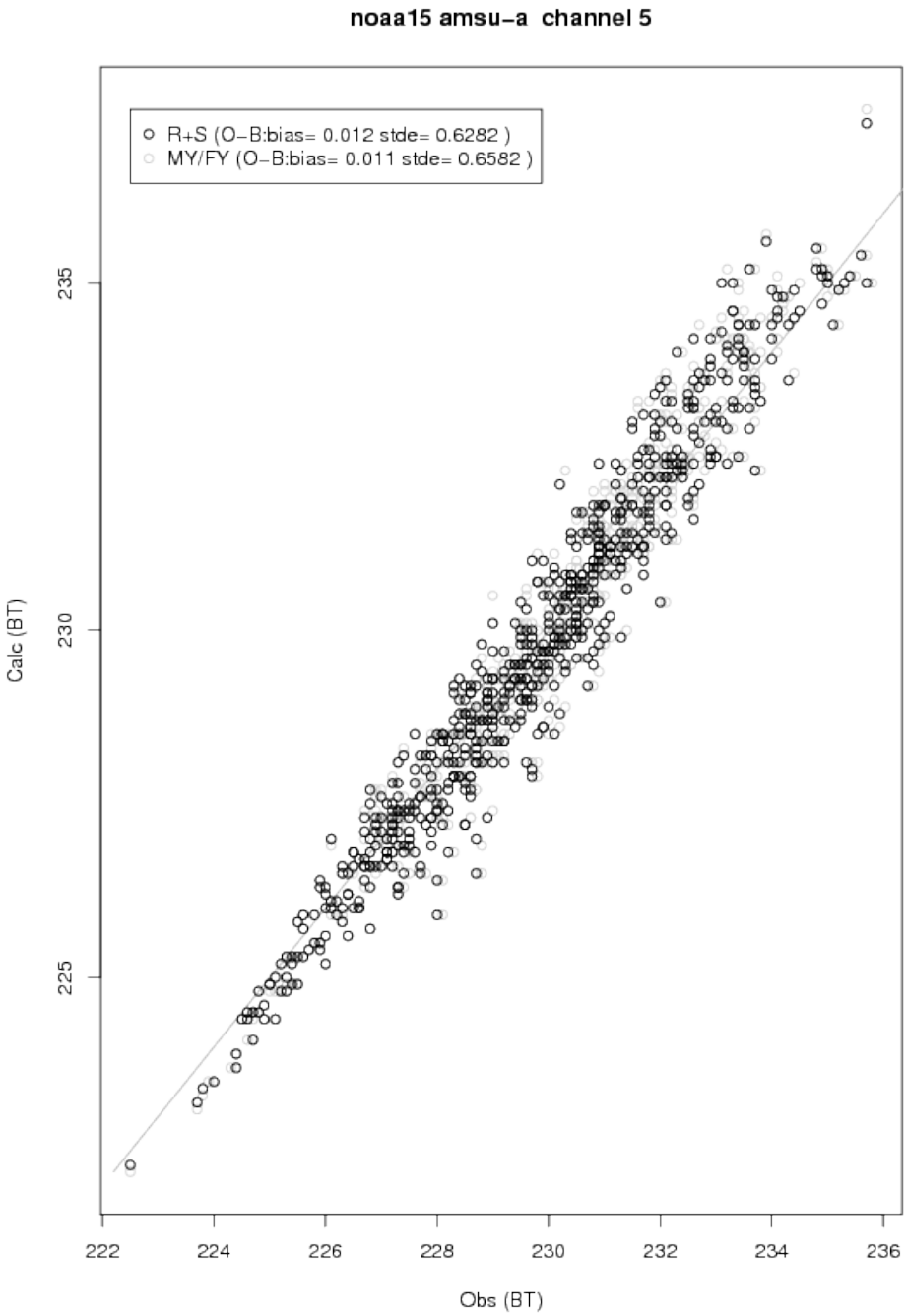

Figure 7: Observed (bias corrected) vs. simulated AMSU-A channel 5 brightness temperatures using the two approaches for emissivities: R+S (OSI SAF) and MY/FY (Heygster et al). Data is for the period 19 Oct to 30 Nov 2011.

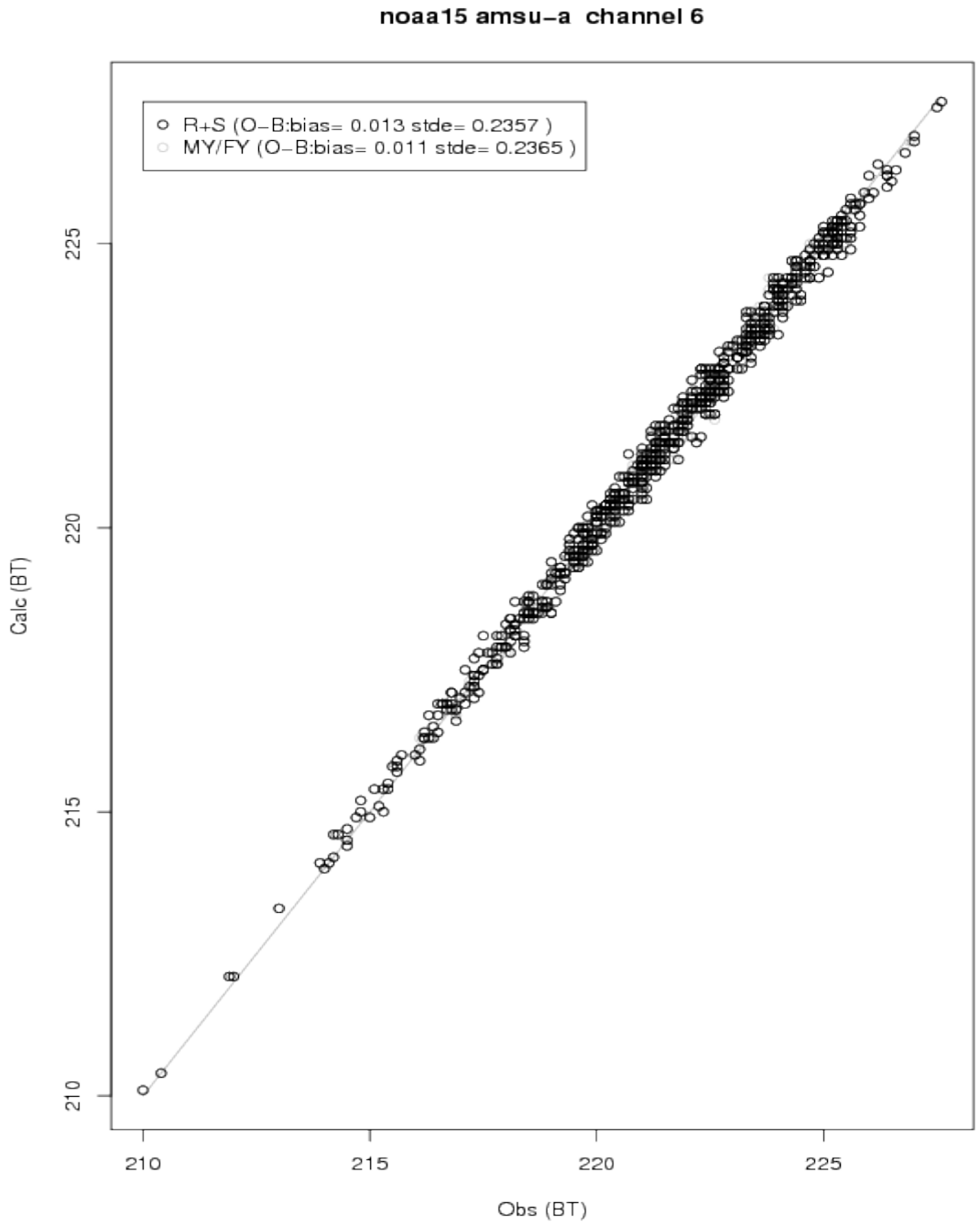

Figure 8: Observed (bias corrected) vs. simulated AMSU-A channel 6 brightness temperatures using the two approaches for emissivities: R+S (OSI SAF) and MY/FY (Heygster et al). Data is for the period 19 Oct to 30 Nov 2011.

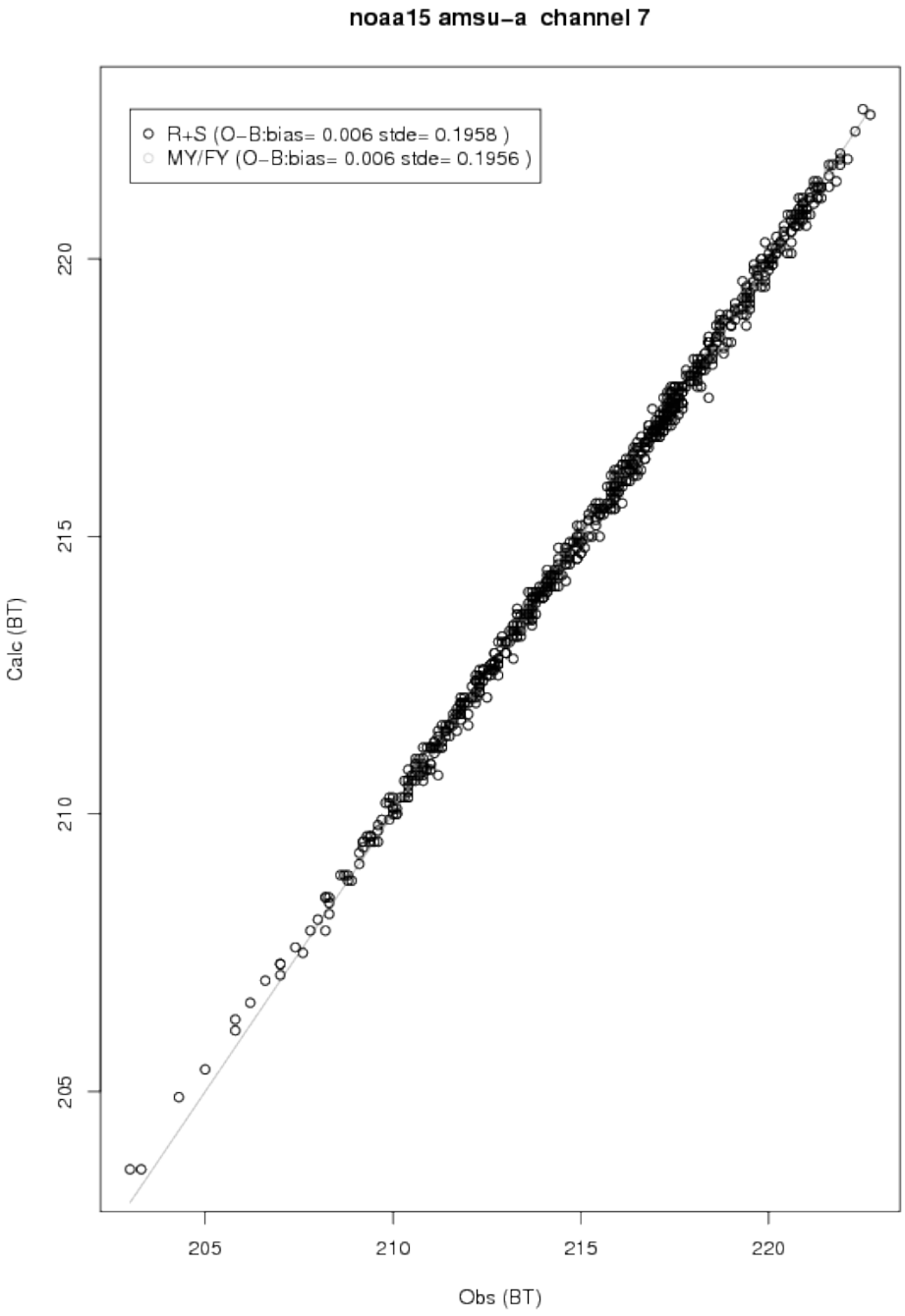

Figure 9: Observed (bias corrected) vs. simulated AMSU-A channel 7 brightness temperatures using the two approaches for emissivities: R+S (OSI SAF) and MY/FY (Heygster et al).

We generally see a slightly better fit to the observations with the OSI SAF emissivities in the plots. One way of quantifying the scatter is with the standard deviation of error (STDE), calculated from the simulated minus observed values. We have summarized the results in terms of this measure of scatter in Table 1.

	NOAA-15 FY/MY	**NOAA-15 R+S**	**NOAA-16 FY/MY**	**NOAA-16 R+S**
Channel 3	5.5844	**3.9544**	5.4543	**3.975**
Channel 4	1.7597	**1.5371**	-	**-**
Channel 5	0.6582	**0.6282**	0.6542	**0.6251**
Channel 6	0.2365	**0.2357**	0.2155	**0.2132**
Channel 7	0.1956	**0.1958**	0.2699	**0.2699**

Table 1: Standard deviation of departures in Kelvin between the simulated AMSU-A observations with the two emissivity models and bias corrected observations. Data is for the period 19 Oct to 30 Nov 2011. FY/MY: Using multi-year fraction as predictor (Heygster et al in [RD.2]). R+S: The OSI SAF product. The two columns to the left are for NOAA-15, the two to the right for NOAA-16. Channel 4 on NOAA 16 is not functioning.

Figure 10 shows a similar scatter plot (simulated versus real observations) for the dynamical emissivity method for channel 5. This could be compared to Figure 7 above, and it seems that the scatter is less. We do not show scatter plots for the rest of the channels with the dynamical method here, but a summary of the fit to observations in terms of RMS errors for all channels of interest when using this emissivity method is given in Table 2. Here the results for the OSI SAF R+S method has been repeated for reference. For the strongly surface affected channels the fit with the dynamical method is better, but the R+S method becomes comparable for channels where the atmospheric contribution is higher. Regarding the "perfect" fit of the dynamical method in channel 3, this is by design of the method: The dynamical method determines the emissivity by adapting emissivity to make the simulated observation exactly match the actual observed value in channel 3.

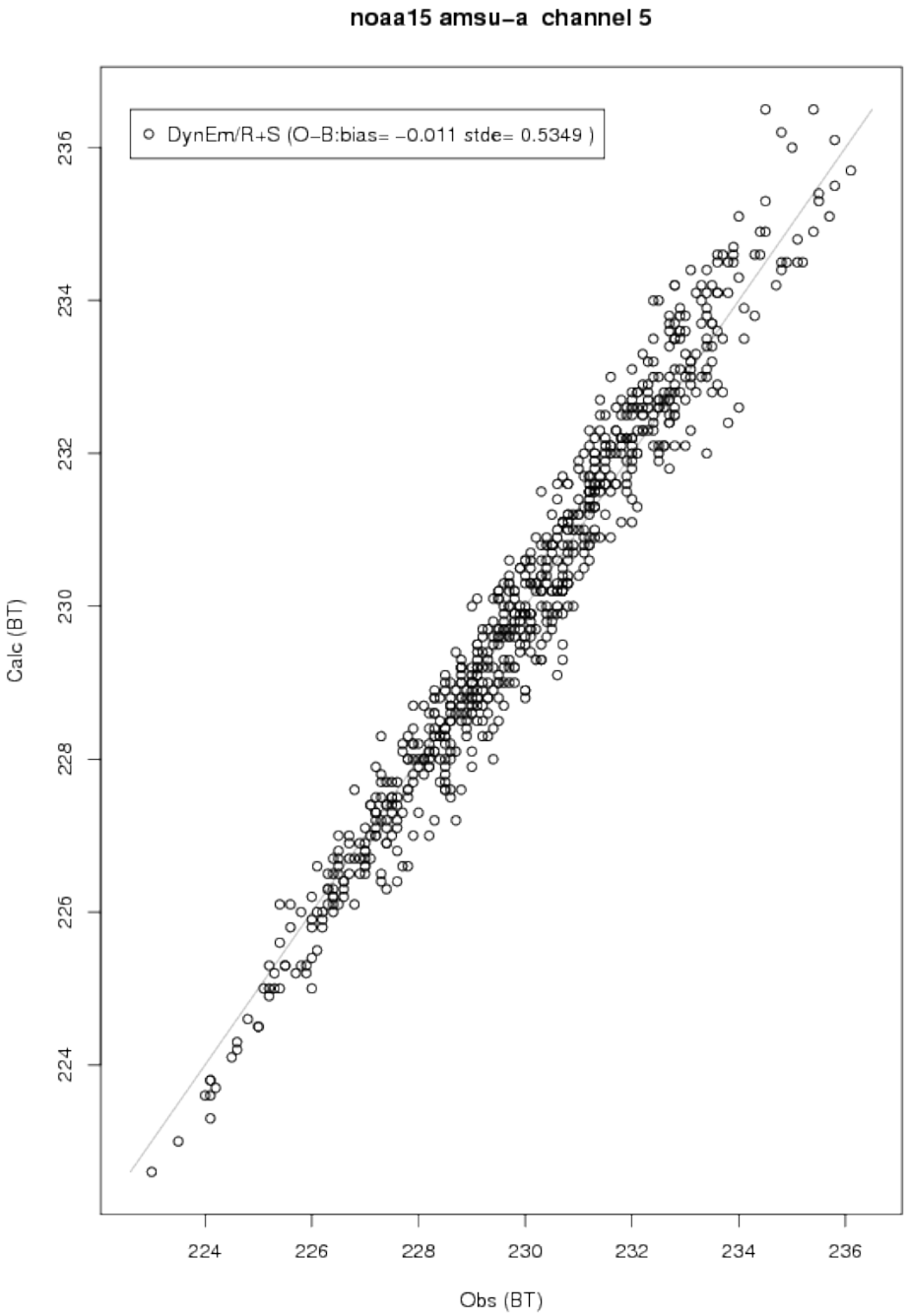

Figure 10: Observed (bias corrected, horizontal axis)) vs. simulated (vertical axis) AMSU-A channel 5 brightness temperatures using "dynamical" emissivity based on channel 3.

Inaccuracies in emissivity is only one of several reasons which can cause misfit between observations as outlined in Section 3. This means that the emissivity estimate calculated with the dynamical method also will make the observation fit if there are other causes than emissivity contributing, such as representativeness errors or other observation errors. This can explain the fact that emissitivites greater than 1 are seen in Figure 5 when emissivities were derived with the dynamical method. If the dynamical method compensates this type of observation uncertainty it could be regarded as an asset if these errors in channel 3 were the same as in the other channels. However, since there is not a perfect correlation of uncertainty between different channels, the methodology may be introducing new errors or compensate in the wrong way.

There can also be a component from the error in atmospheric information from HIRLAM contributing to the emissivity estimate. The primary contribution to the signal is from the surface in the AMSU channel 3 (50.3 GHz). However, there is also a small contribution to the signal from the atmosphere and therefore the emissivity estimate from the dynamical method is slightly adjusted to compensate if there are errors in the lower part of the atmospheric profile from HIRLAM. This departure is part of the signal which we wish to exploit in the NWP data assimilation. Since the same atmospheric signal also affects the Tb's at other lower-tropospheric channels applying the same emissivity, a part of the good fit is obtained by also removing atmospheric signal that we are interested in.

It is therefore encouraging that the fit with the OSI SAF method, which provides an independent estimate, is comparable or better than the dynamical method for channels dominated by atmospheric emission.

	NOAA-15 Dyn (ch3)	**NOAA-15 R+S**	**NOAA-16 Dyn (ch3)**	**NOAA-16 R+S**
Channel 3	0	**3.9544**	0	**3.975**
Channel 4	0.8592	**1.5371**	-	**-**
Channel 5	0.5349	**0.6282**	0.5559	**0.6251**
Channel 6	0.2317	**0.2357**	0.2153	**0.2132**
Channel 7	0.2007	**0.1958**	0.2677	**0.2699**

Table 2: Standard deviation of departures in kelvin between the simulated AMSU-A observations with the two emissivity models and bias corrected observations. Data is for the period 19 Oct to 30 Nov 2011. Dyn: Using "dynamical" emissivity calculated from channel 3. R+S: The OSI SAF product. The two columns to the left are for NOAA-15, the two to the right for NOAA-16. Channel 4 on NOAA 16 is not functioning.

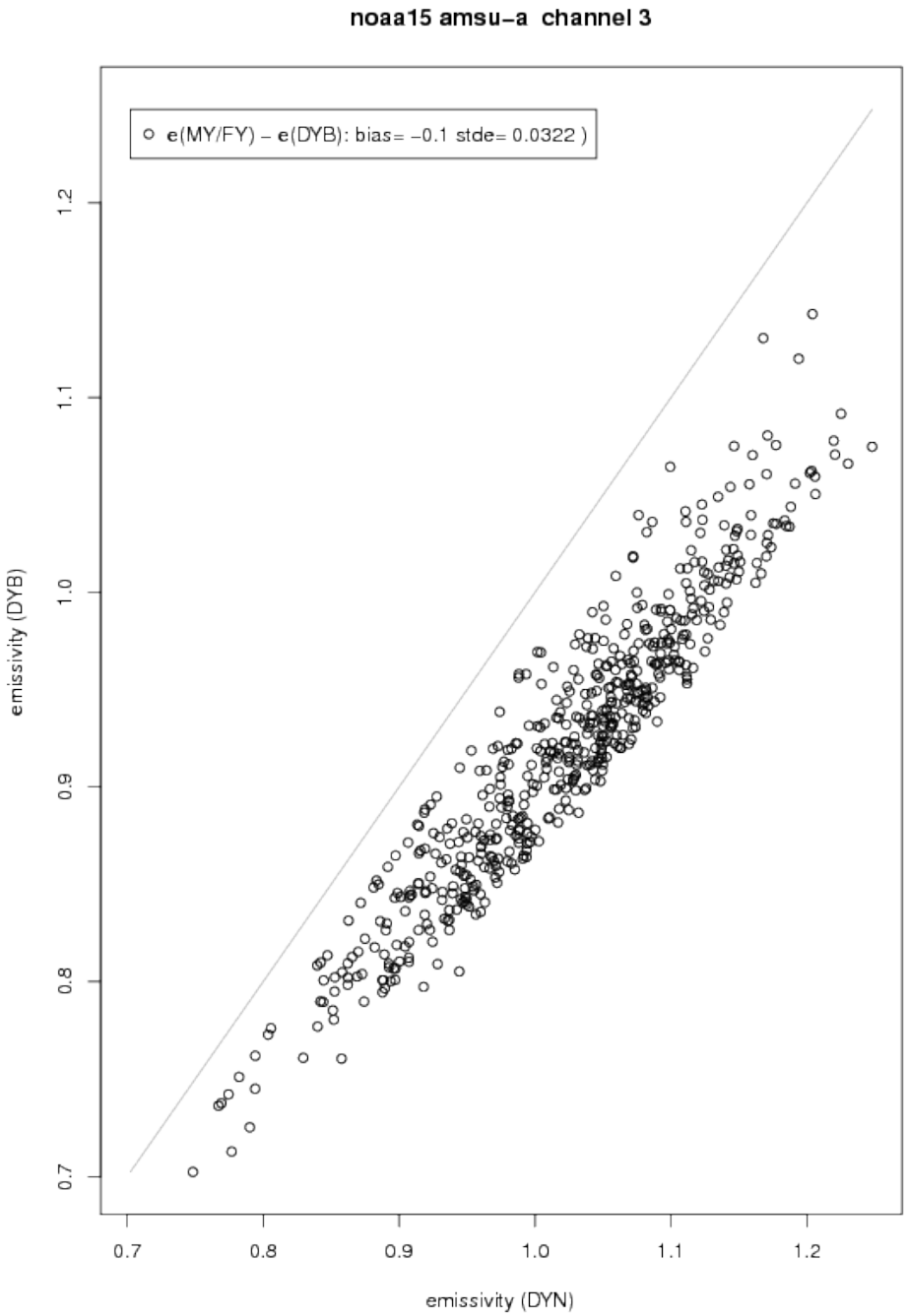

Figure 11: Comparison between emissivities calculated using the dynamical method based on channel 3, vertical axis: from calculations using bias corrected brightness temperatures, horizontal axis: from calculations using raw uncorrected brightness temperatures. (NOAA-15, period 1 November-31 December 2011).

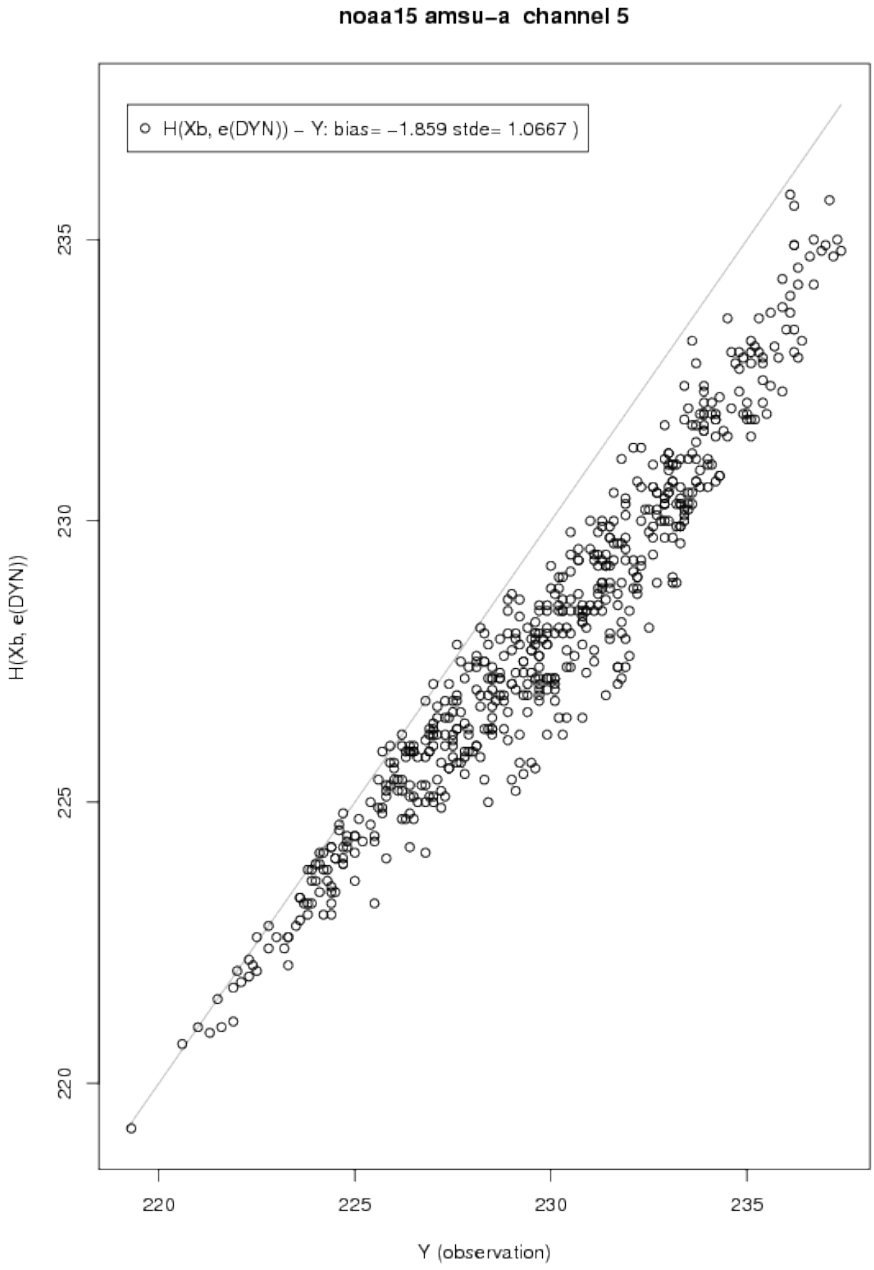

Figure 12: Comparison between observed and simulated brightness temperatures for NOAA-15 AMSU-A ch5 using dynamic emissivity based on *non-bias-corrected* data. To be compared with next figure. This comparison is for the period 1 November-31 December 2011.

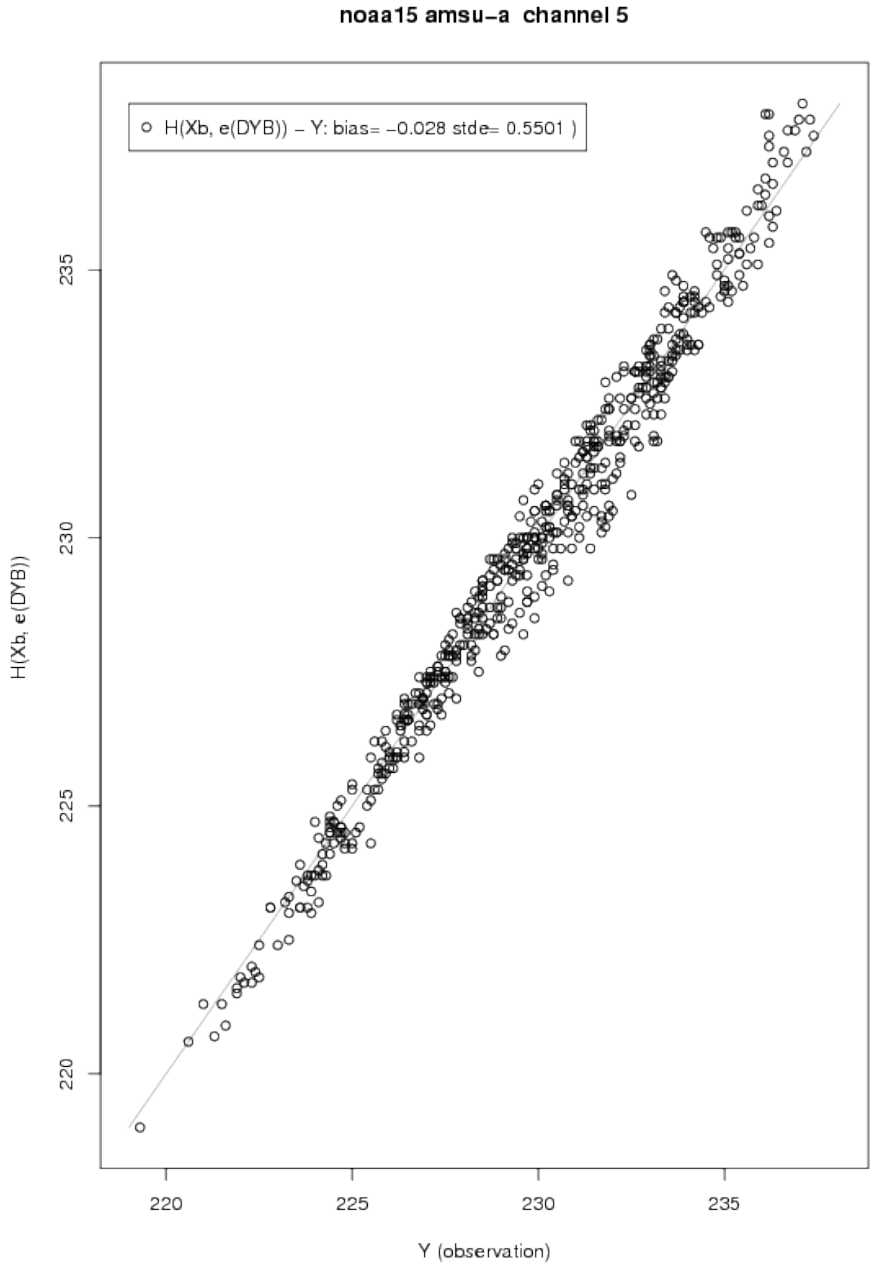

Figure 13: Comparison between observed and simulated brightness temperatures for NOAA-15 AMSU-A ch5 using dynamic emissivity based on *bias-corrected* data. To be compared with previous figure. This comparison is for the period 1 November-31 December 2011.

7. Conclusion for the R and S validation method

The differences between the OSI SAF emissivity product and the MY based emissivity product have been discussed and the reasons for these differences seems well understood. The R and S method is able to simulate emissivities for both the vertical and the horizontal polarisation and for incidence angles between 0 and 60 deg. Both the OSI SAF method and the multi-year fraction based method use the relationship between the spectral gradient at 19 and 37 GHz and the 50 GHz emissivity and the correlation between the two methods is high. The simulated AMSU-A observations based on the OSI SAF emissivity model and HIRLAM data gives generally a comparable or better fit to the corresponding real observations than when using multi-tear fraction approach for emissivity.

Regarding comparison with the dynamical method for emissivities, it is not unexpected that this method gives better fit to the data than using the OSI SAF emissivities. This method essentially adapts the emissivity to make it fit the observation in channel 3 when using the HIRLAM data, so it is an optimal choice for fitting the data based on this channel. But the method will also implicitly use the emissivity to adjust for errors in the HIRLAM input data contributing in channel 3. Since these errors or signals also affect the other channels, a very good fit is obtained, however at a risk of also removing some of the atmospheric signal that we look for to correct the NWP model when using temperature sounding channels.

The validation method chosen here is not suited to assess how much atmospheric signal is removed with the dynamical method. For a more complete assessment of that, it could have been interesting to perform NWP assimilation experiments with AMSU-A data comparing the two emissivity methods and compare the effect of the two methods on forecast skill, but this has not yet been possible within the frame of the project. It is very encouraging that the fit to the data with the OSI SAF method is comparable to the dynamical method in channels 6 and 7.

We conclude that the OSI SAF emissivity product is technically well implemented and physically behaves as expected. We have pointed out the methodological problems in making an exact estimate of the accuracy of an emissivity product. In the comparison of the SAF product with well known alternative ways of deriving emissivity, the standard deviation of differences between the various methods were less than 5%. This is an indication that the product at least is within both the threshold (0.15) and target (0.05) accuracies defined in the Product Requirements Document [RD.6].

The OSI SAF emissivity product is very well able to help model the surface contribution to 50GHz sounding channels. It has the advantage compared to the dynamical method of using information independent of the AMSU measurements themselves to describe the surface, so there is no risk of removing atmospheric signals when using the product.

8. The continuous near 50 GHz sea ice emissivity validation

The microwave sea ice emissivity is not measured by any space borne, airborne or in situ devices. Anyway, it affects the thermal microwave emission from the sea ice surface and the top-of-the atmosphere microwave brightness temperature measured by satellites. The near 50.3 GHz and 52.8 GHz channels on a number of atmospheric sounders for example the SSMIS, which is used here, are on the

shoulder of the atmospheric oxygen absorption line complex and while the surface emissivity is the same at the two channels they are affected very differently by the intervening atmosphere. The notation for the brightness temperatures is, for example, Tv50 meaning the 50.3 GHz brightness temperature at vertical polarisation. The surface emissivity is denoted e. Here e means the vertically polarised emissivity at an incidence angle of 53.1 degrees. A simplified radiative transfer equation describes the atmospheric and surface emission interaction, so that the brightness temperature, *Tb*, measured by satellite is:

$$Tb = TBU + \tau(eT_{eff} + (1-e)TBD) \qquad \text{(eq.2)},$$

where *TBU* is the up-welling radiances from the atmosphere, τ is the atmospheric transmissivity, T_{eff} is the surface effective temperature, *e* is the surface emissivity, and *TBD* is the down-welling atmospheric radiance. Here we wish to estimate e using the Tv50 and the Tv52 SSMIS data, NWP data on temperature and water vapour, for comparison with the OSI SAF near 50 GHz sea ice emissivity product. The emissivity product is computed using a forward model and the correlations between neighbouring channels.

8.1. The validation product procedure

In essence, the e is estimated iteratively by minimizing the difference between Tb's measured by SSMIS and simulated *Tb's* at 50.3 GHz vertical polarisation and the 52.8 GHz vertical polarisation using equation 2 and given the water vapour and temperature of the atmosphere from the ECMWF numerical weather prediction model (current near real time operational model [RD.10]). SSMIS is a conical scanning radiometer measuring at a constant incidence angle of 53.1 degrees. In the product NetCDF file the emissivity variable is called *ev* and it is the surface emissivity at vertical polarisation and at 53.1 degrees of incidence angle. This continuous validation procedure is in many ways similar to the initial and much shorter period validation of the emissivity product which is described earlier in this validation report and in Tonboe et al. (2013) [RD.8]. However, this continuous validation procedure is much more computationally efficient which allows real time validation globally on every ice covered pixel. The four step procedure is:

1. Input data are: SSMIS Tv50 and Tv52, ECMWF total water vapour, and surface air temperature.
2. All of the variables in equation 2 except the *e* are computed based on the input data and a regression RTM [RD.9].
3. The emissivity, e, is found iteratively using the local adjoint of equation 2. The scheme is solved using two different first guess emissivities and the physical and radiance covariance for constraints.
4. The OSI SAF emissivity and the *e* bias and STD is computed and illustrated in scatterplots and in geographical plots.

The effective surface temperature (*Teff* in eq. 2) is computed as a linear mix between the surface air temperature (*Ta*) and the freezing point of sea water (Tw) at 271.35K. We are using the slope from Mathew et al., (2008) [RD.4] for 50GHz. However, the Mathews equation is physically inconsistent for air temperatures near 0°C so the following equation is used instead, i.e.

$$T_{eff} = 0.3T_a + 0.7T_w \qquad \text{(eq. 3)}.$$

Mathew et al. (2008) will have a cold bias in Teff for temperatures near 0°C. Our equation 3. will find Teff between the surface air temperature and the freezing point of sea water.

8.2. The continuous validation results

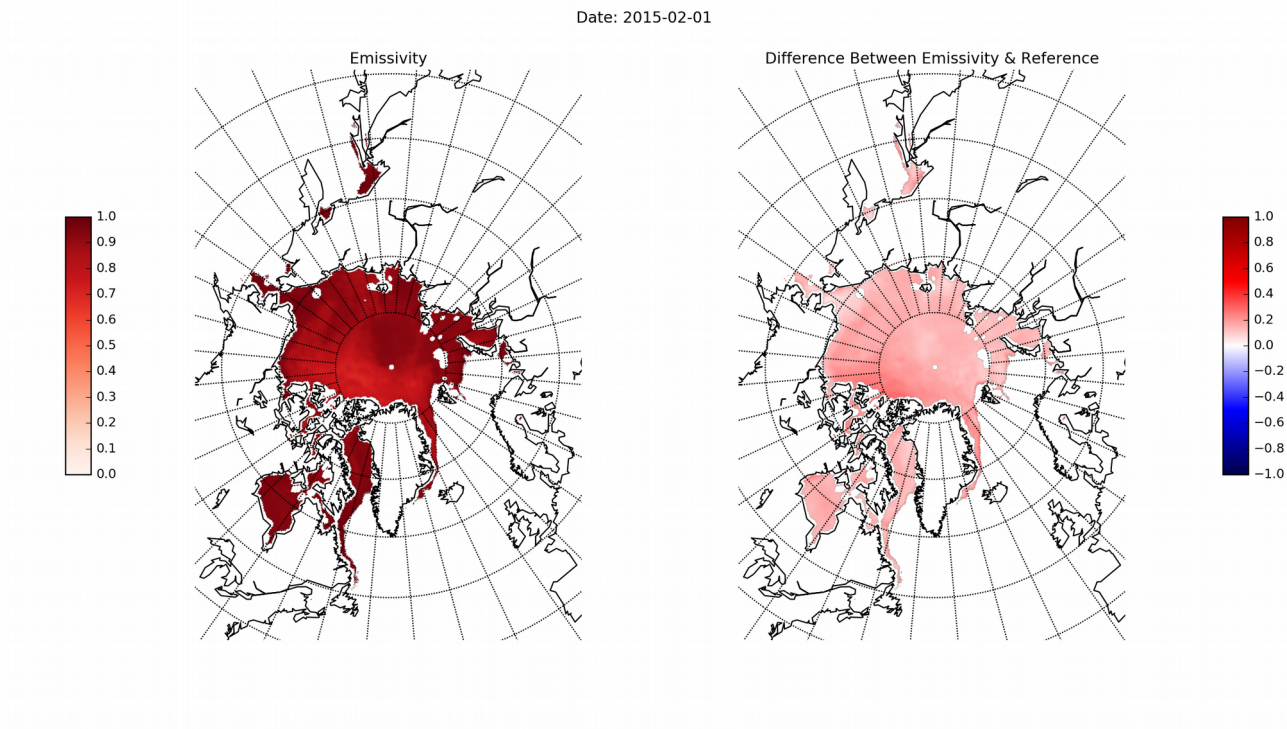

Figure 14: The Northern Hemisphere product emissivity (left) and the bias (product – validation reference emissivity difference) for a day in the calendar year 2015.

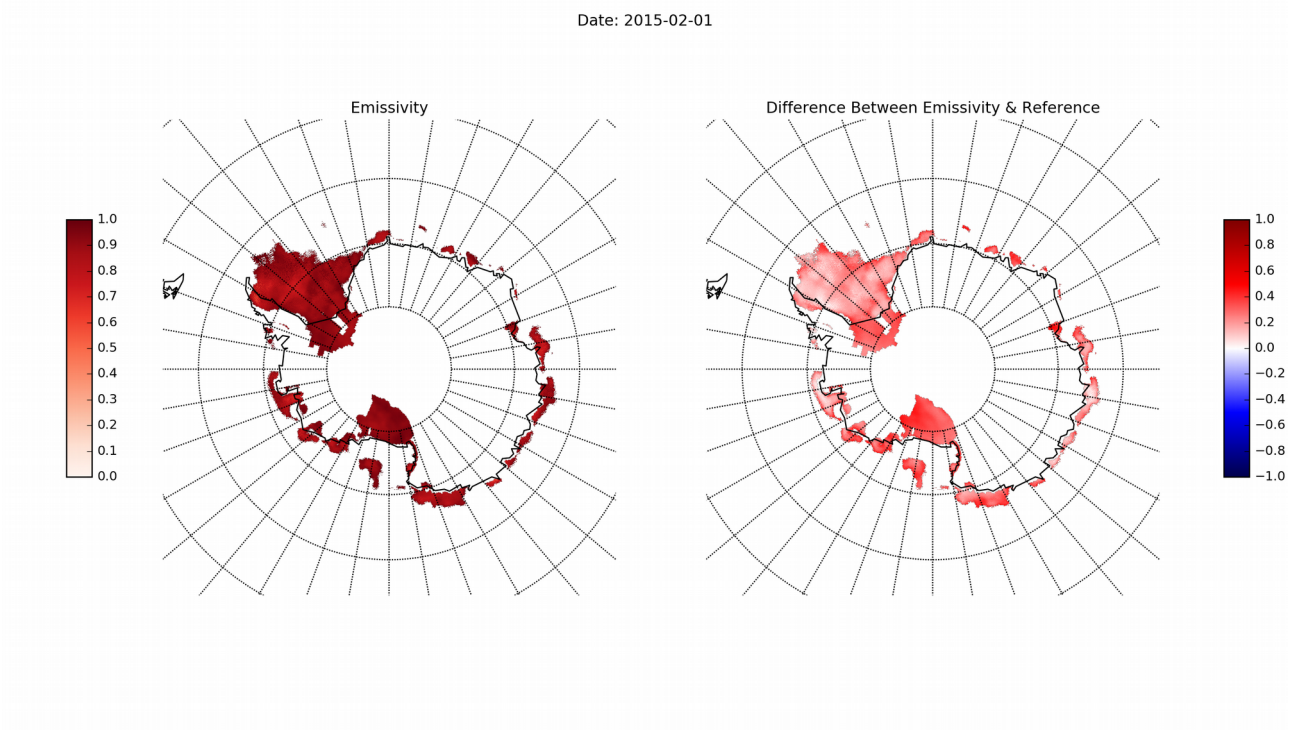

Figure 15: The southern hemisphere product emissivity (left) and the bias (product – validation reference emissivity difference) for a day in the calendar year 2015.

The continuous validation has been reprocessed globally for the calendar year 2015. Figures 14 and 15 are showing first the product emissivity geographically for both hemispheres to the left and then the bias between the product emissivity and the validation reference emissivity to the right. It is clear that the bias is larger over multiyear ice on the northern hemisphere or over thick ice covered by deep snow on the southern hemisphere. Also the ice shelves in Antarctica have a larger bias. The bias is relatively small for regions covered by first-year ice and ice during surface melt. The bias is primarily caused by too warm Teff over thick ice which is resulting in too low validation reference emissivities ($Tb=e*T_{eff}$). The T_{eff} is the integrated emitting layer temperature and here we use a model for the T_{eff} where it is a linear combination of the air and the water temperature. This model does not take account for variability of snow and ice thickness, thermal conductivity of the snow and ice and the penetration depth in different ice types. These parameters are in general not available on a daily timescale and a specific evaluation differentiating between the ice/snow types is not possible at the moment. The emissivity bias for first-year ice is around 0.1 and for multiyear ice it is 0.2. In the next update of the OSI-404 there will be an estimate of T_{eff} using a more sophisticated model and then we expect the bias to be reduced. Anyway, the metric that we use for comparing the product with the validation reference, the metric in the product requirements document is the standard deviation,STD, of the difference between the product and the reference and not the bias, i.e.

$$std = \sqrt{\left(\sum (xi - x)^2 / (N-1)\right)} \quad \text{eq.4,}$$

xi is the difference between the product and the validation product, x is the mean difference between the product and the validation product, and N is the number of observations.

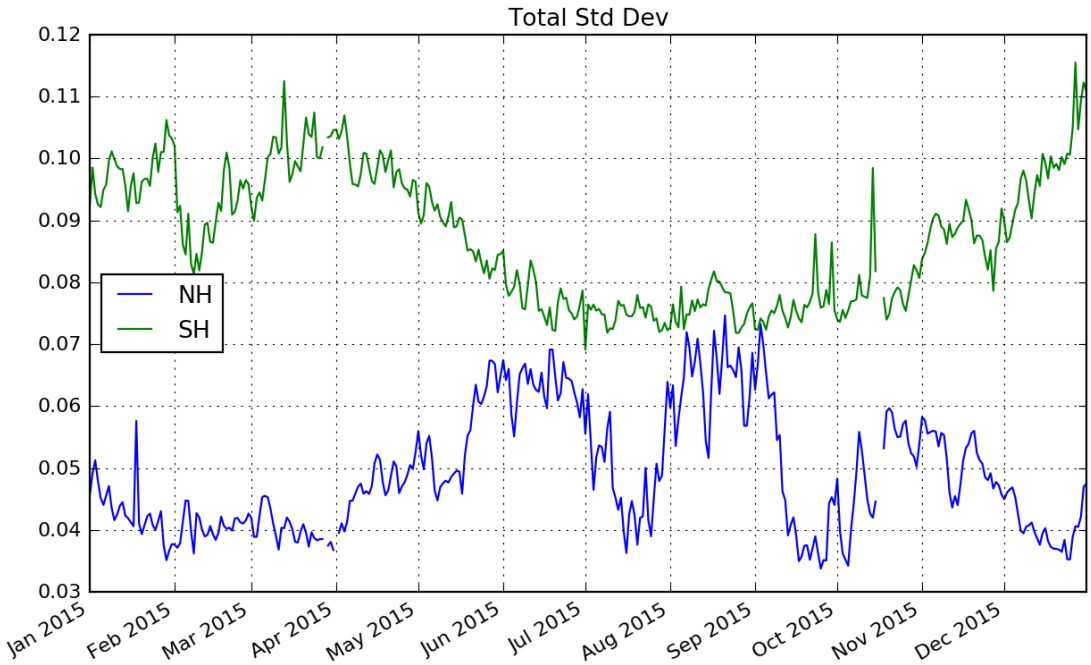

Figure 16: The standard deviation of the difference between the hemispheric average product emissivity and the validation reference emissivity for the southern (SH) and the northern (NH) hemispheres for the calendar year 2015.

The average standard deviation (STD) of the difference between the hemispheric product emissivity and the validation reference emissivity is shown for 2015 with the green (SH) and blue (NH) curve in figure 16. On the southern hemisphere the STD (the metric for evaluating the product) is at all times smaller than 0.12 and on the northern hemisphere smaller than 0.08. The is smaller than the target metric described in the PRD [RD.11] at 0.15 and 0.10. The STD on the southern hemisphere is at all times greater than the STD on the northern hemisphere. On the SH the STD in (Austral) summer (here Nov.-May) is between 0.08 and 0.12 and during the winter (here Jun. - Oct.) it is between 0.07 and 0.08. On the northern hemisphere the STD is more variable across the season with STD's around 0.04 during Arctic winter (here Dec. – Mar.) and up to 0.07 during summer melt. The STD of the difference is due to uncertainties in both the product emissivity and the validation reference emissivity.

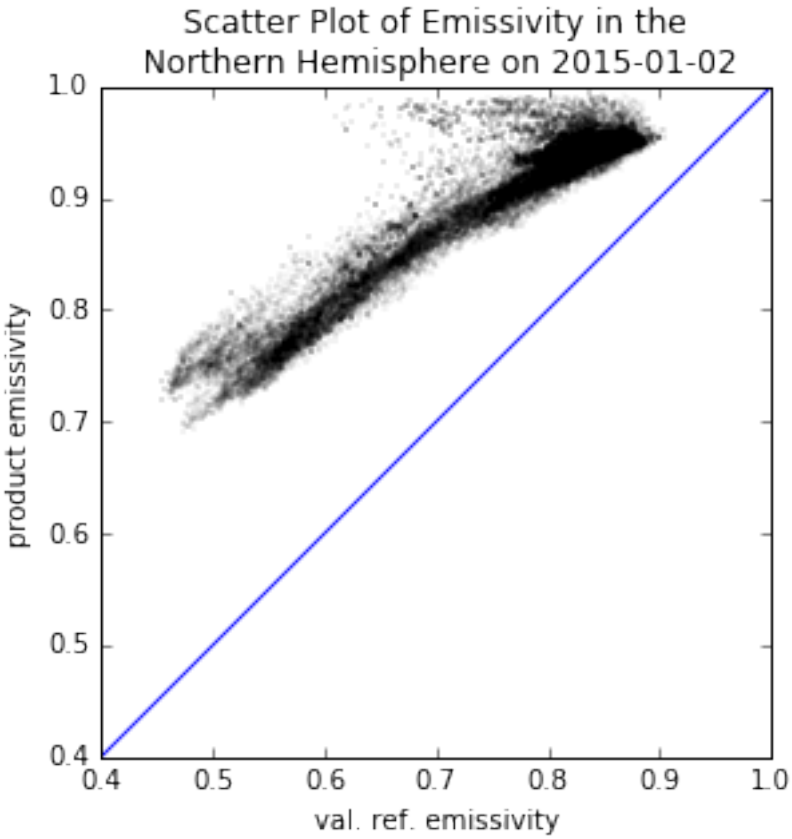

Figure 17: The scatterplot showing the validation reference emissivity vs. the product emissivity on the Northern hemisphere on one particular day (2015/01/02).

Figure 17 shows the scatterplot of the validation reference emissivity vs. the product emissivity on the Northern hemisphere on one particular day (2015/01/02). For all data-points there is a warm bias (product emissivity > validation reference emissivity). The bias is smaller at high (first-year ice) emissivities and larger at low emissivities (multiyear ice).

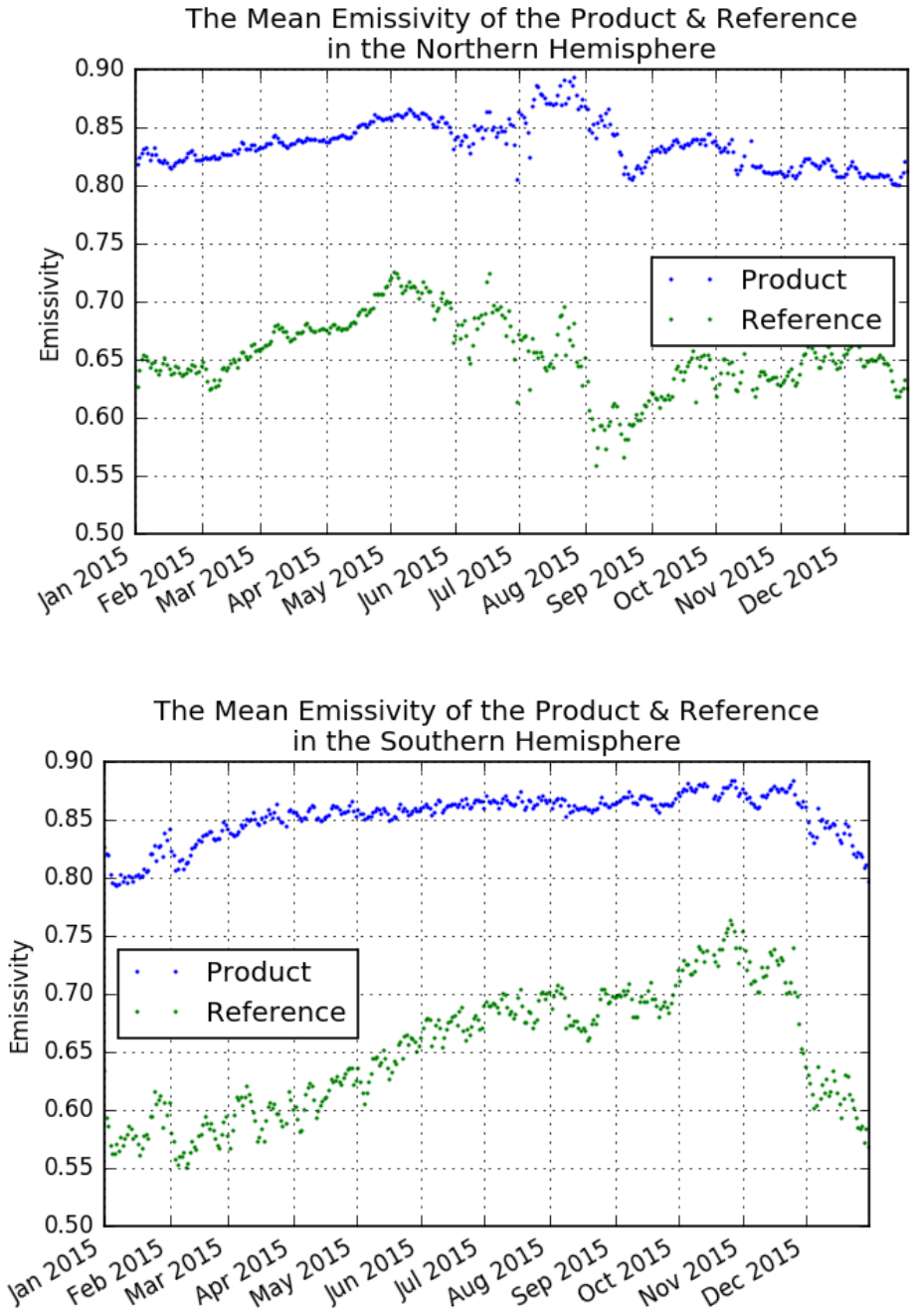

Figure 18: The hemispheric emissivity for both hemispheres for the Northern Hemisphere (top) and Southern Hemisphere (bottom).

Figure 18 shows the hemispheric emissivity for both hemispheres. In spite of the biases between the product and reference it is seen that the seasonal variation follow the same pattern. In general the emissivity increase during early melt.

8.3. Update of the effective temperature in the continuous validation and algorithm coefficients

The estimate of the effective temperature and the product emissivity algorithm coefficients have been updated in order to reduce the bias between the product emissivity and the reference emissivity.

The new S coefficients are:
North: S=2.764*GR1836+0.8624
South: S=2.6438*GR1836+0.8426

The new effective temperature estimate Teff is a function of 6 and 10 GHz brightness temperatures using the equation:

Teff=1.34*T6V + 0.05*T10V – 91.49

The equation has been estimated using the buoy data in the ESA sea ice CCI round robin data package: http://www.seaice.dk/RRDB-v2

Using the new product algorithm coefficients and the new reference effective temperature the bias is reduced as seen in figure 19.

Figure 19:The hemispheric bias between the product emissivity and the reference emissivity (ev) at 53.1 deg incidence angle January to November 2017.

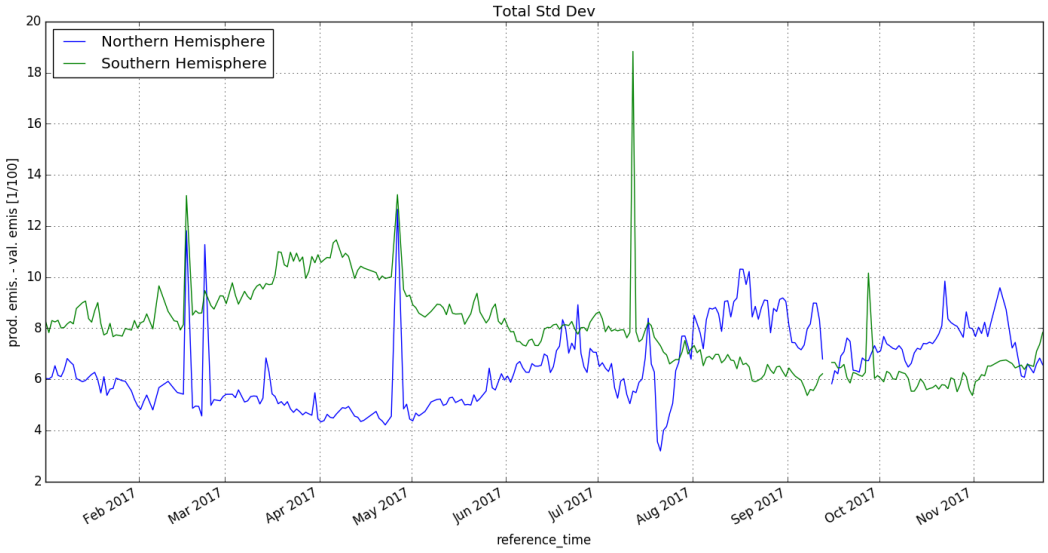

Figure 20:The standard deviation of the difference between the product emissivity and the reference emissivity for each hemisphere.

8.3.1. The sea ice emissivity uncertainties

The sea ice emissivity uncertainties, s, are computed as a 3 by 3 pixel STD of the difference between the product and validation product emissivities, i.e.

$$s=\sqrt{\left(\sum (yi-y)^2/n\right)} \quad \text{eq.5}$$

where yi is the product and validation difference, y is the mean difference, and n is the number of pixels within the 3×3 box (9).

The relatively small 3×3 window was selected to avoid systematic spatial differences between the two products to influence the result. This is a local uncertainty on every pixel. The hemispheric product and validation product STD is including potential biases between the two products. These two measures are not expected to be at the same level. In figure 21 the northern hemisphere uncertainty and the product emissivity and validation product difference STD are shown together. The seasonal variation is similar in both the uncertainty and the product difference STD. They are both low in the winter and higher during summer melt. This shows that the uncertainties are higher during summer than during winter.

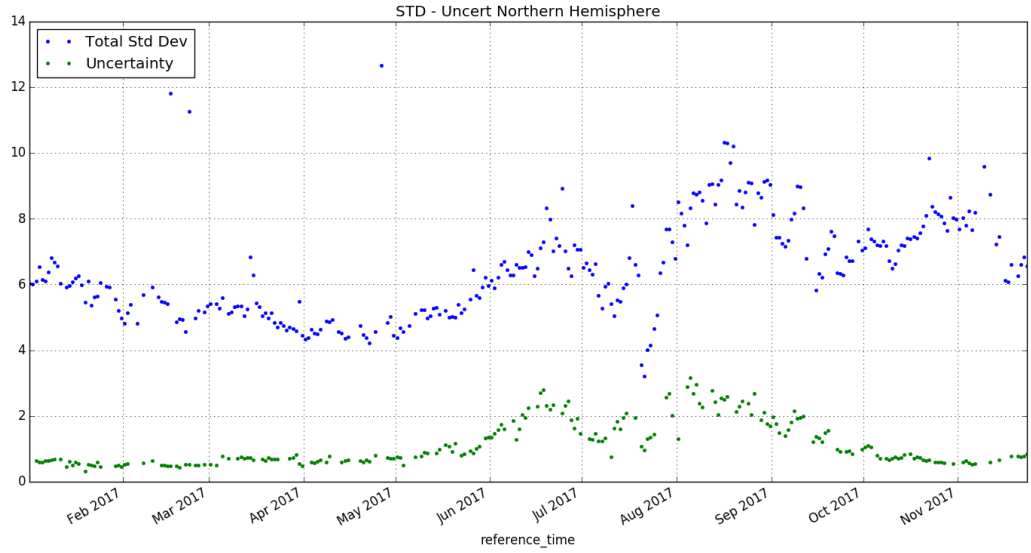

Figure 21: The northern hemisphere uncertainty (green) and the STD if the emissivity (blue).

The uncertainties on the northern and southern hemisphere are similar as shown in figure 22. During winter the uncertainties are close 0.6 and during summer they reach values near 2.5. The transition from summer to winter and from winter to summer is gradual on both hemispheres.

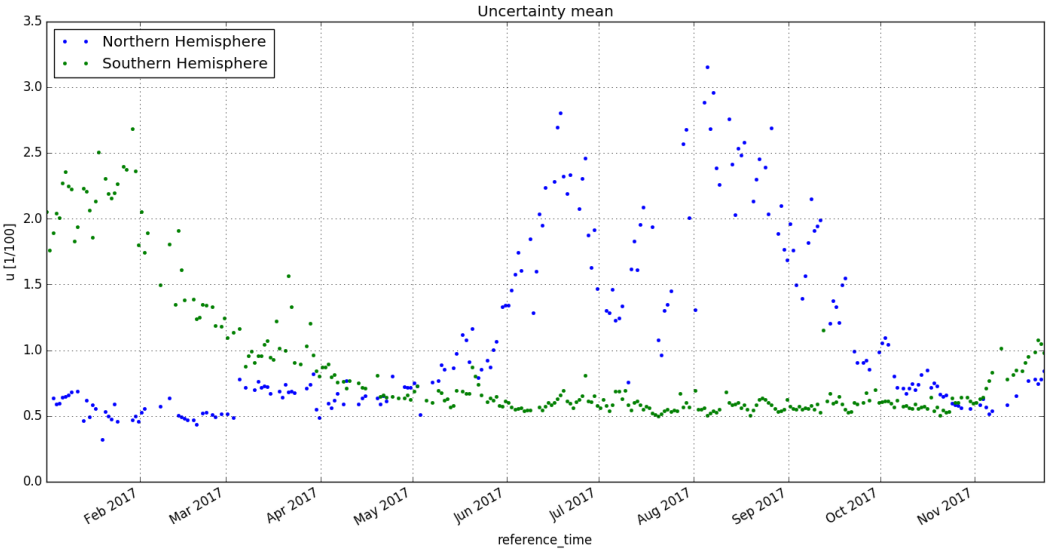

Figure 22: The uncertainty is shown for the northern hemisphere and the southern hemisphere for the 11 months of 2017.

9. Concluding remarks for the continuous near 50 GHZ validation

The product emissivity and the validation reference emissivity difference could be minimized by tuning the model for computing the T_{eff} and by making it a function of ice type. This would to some extent also reduce the STD of the difference between the product and the validation reference emissivities. Both emissivity datasets have uncertainties. The uncertainties of the validation reference are related to RTM model uncertainties i.e. biases in the up- and down-welling radiances and in the T_{eff} model. The sea ice effective temperature is a function of the surface temperature, the snow and ice thickness, snow and ice thermal conductivity, snow and ice morphology. None of these parameters are well known on large scale and we therefore use a simple empirical model for T_{eff}. There are also uncertainties in the representation of the NWP air temperature and water vapour and cloud liquid water is not included in the calculation because NWP cloud liquid water does not have sufficient accuracy for explicit correction. There are also uncertainties related to the daily variability and resampling. The product emissivity uncertainties are related to the algorithm uncertainties, to atmospheric noise which is not corrected because we do not want to introduce biases from the NWP model in the product and to daily variability and resampling.

It is concluded that the OSI SAF emissivity product is technically well implemented and physically behaves as expected. The methodological problems in making an exact estimate of the accuracy of an emissivity product has been pointed out. After updates of the effective temperature estimate in the reference emissivity and the coefficients in the product algorithm the bias has been minimized (Section 8.3). The fact that the product and the reference are two different and independent products gives a small bias and a SD of the difference. However, there is no large systematic bias. In the comparison of the SAF product with validation reference emissivity, the standard deviation of differences between the various methods were less than 10% on the NH and less than 15% on the SH. This is below the PRD [RD.11] target threshold at 15% in the NH and SH.

The variability of the OSI SAF product is at the same level as before the update of coefficients. However, the validation product has changed with the continuous validation procedure. The OSI SAF and the continuous validation product are independent products and that comparison gives different results than what was achieved in the first much more limited validation.